ELSEVIER

Journal of Alloys and Compounds 229 (1995) 40–53

Journal of ALLOYS AND COMPOUNDS

Exploring the metal-rich chemistry of the early transition elements

Timothy Hughbanks

Department of Chemistry, Texas A&M University, College Station, TX 77843-3255, USA

Received 20 April 1995

Abstract

The early transition metals, especially Zr, Hf, Hb and Ta, exhibit a metal-rich chemistry that is often surprising in its structural and physical aspects. Unfamiliarity with this chemistry is illustrated by the discovery of several new binary compounds in the Ta–S, Ta–Se, Ta–Te, and Hf–Te systems within the past few years. Some striking differences observed between the metal-rich chalcogenides of Zr and Hf or between Nb and Ta challenge basic presumptions about the similarity of these congeneric pairs. The factors controlling the structural anisotropy of a new class of tetragonal layered compounds that includes Ta_2Se, $Ta_{2-x}Nb_xS$, Hf_3Te_2, and ZrZTe (Z ≡ Si, Ge, Sn) are discussed. Strongly early–late transition metal intermetallic bonding leads to the formation of an expanding class of compounds that includes $Ta_9M_2S_6$ (M ≡ Fe, Co, Ni), $Ta_{11}M_2Se_8$ (M ≡ Fe, Co, Ni), Ta_8NiSe_8 and the newly discovered hafnium tellurides, Hf_8MTe_6 (M ≡ Mn, Fe, Co, Ni, Ru) and Hf_5MTe_3 (M ≡ Fe, Co). Our efforts to dismantle solid-state Zr–halide cluster compounds is described. Ambient temperature molten salts help us achieve the controlled excision of $[(Zr_6Z)CL_{18}]^{n-}$ from solid state precursors; we describe the applications of electronic and NMR spectroscopies in characterizing clusters in solution. Finally, we discuss bonding in metal-rich systems, with particular emphasis on localized bonding descriptions for metal–metal bonds in extended metal-linked networks. Such localized descriptions increase our understanding of otherwise anomalous properties and illuminate the artificiality of separate "metallic" and "covalent" bonding concepts.

Keywords: Metal-rich chemistry; Early transition metals

1. Metal-rich material

The field of metal-rich chemistry, when it is thought of as "chemistry" at all, remains outside the experience and conceptual framework of most chemists. Instead, the reaction chemistry of metal-rich compounds has often been relegated to metallurgists, while the study of these compounds' physical properties has been left to the field of "metals physics". We believe that, with notable exceptions, this has led to a strongly distorted view of the breadth of metal-rich chemistry, the nature of the "metallic bond", and of the potential for metal-rich compounds to do "interesting chemistry". In this article, some of the principal themes that drive research in our group at Texas A&M are discussed, including examples from the synthesis of early metal chalcogenides, the reaction chemistry of zirconium halide clusters, and analyses of bonding in systems that help to illuminate the still misunderstood "metallic bond".

2. New compounds

2.1. Binaries and Pseudobinaries

Binary, early-transition-metal chalcogenides of surprisingly simple composition continue to be found. Recent attention to this chemistry and advances in synthetic methodology have produced Ta_2Se [1], Ta_3S_2 [2,3], Ta_2Te_3 [4], and Hf_3Te_2 [5]. In addition, Conrad and Harbrecht have discussed the compound Ta_6Te_5 [6], although no details about its preparation or structure have yet been published. It is interesting that binaries with such uncomplicated compositions escaped detection until quite recently. Various reasons can be offered for this state of affairs. Metal-rich compositions may have been examined; however, since crystals of these refractory compounds are difficult to obtain at lower temperatures, it may be that they were simply not characterized. Furthermore, if one attempts the synthesis of these compounds in silica or alumina

SSDI 0925-8388(95)01688-0

containers, the products are badly contaminated with silicides, silicates and oxides. At least some of these new compounds (Ta_3S_2, Ta_6Te_5) melt incongruently and cannot be formed in high temperature reactions that have been used traditionally in exploratory synthetic surveys. Finally, it is possible that investigators have simply assumed that there was little new to find in these systems.

The metal-rich chalcogenides of Zr, Hf, Nb, and Ta challenge basic assumptions about the chemistry of these elements. The pair of elements Zr and Hf are generally believed to be more similar in their chemistry than any other pair of congeneric elements and the similarities of Nb and Ta are nearly as close [7,8]. These pairs of elements have nearly identical radii (atomic or ionic), electronegativities, and elemental structures. Given all this it is rather surprising to find that distinctions exhibited within both pairs of elements are fairly sharp when it comes to their metal-rich chemistry. Let us first consider binary and pseudobinary chalcogenides. (The term "pseudobinary" will be used to describe compounds and involve solid solutions of congeneric transition metals.)

The layered dichalcogenides MX_2 ($M \equiv$ Zr, Hf, Nb, Ta; $X \equiv$ S, Se, Te), are quite familiar, even to the wider community of chemists. In the past 6 years, several surprising (pseudo)binary chalcogenides of these metals have been uncovered that also possess layered structures, but with transition metal contents greater than or equal to 60 at.%. Harbrecht discovered that the first of these remarkable layered compounds, Ta_2Se, could be prepared in a simple arc melting reaction. As depicted in Fig. 1, the robustly metallic layers in this compound consist of four (100) layers of b.c.c. Ta sandwiched between two square nets of Se; these layers are stacked with Se centers of each layer directly opposite Ta atoms of an adjacent layer, but at rather long distances (3.82 Å). In an alternative description, Ta_2Se is formally an insertion compound related to bulk b.c.c. metal. After every four layers of Ta, two layers of Se are inserted. Isoelectronic Nb_2Se has a very different structure [9,10], that has been described as built up from condensed octahedral clusters [11].

Pseudobinary $Ta_{2-x}Nb_xS$ analogs of the Ta_2Se type were soon found in Franzen's laboratories and in our laboratory as well [12,13]. The appearance of this layered structure in the mixed-metal system is striking in that no such layered structures are observed in either the Ta–S or Nb–S systems [14,15]. It appears that the driving force for the formation of this layered structure may be the opportunity that it offers for segregation of the metals. We find that in $Ta_{1.4}Nb_{0.6}S$ almost all the Nb is found in the outermost metal layers of the slab; X-ray refinements indicate that only about 5% of the inner-layer metal atoms are Nb. We

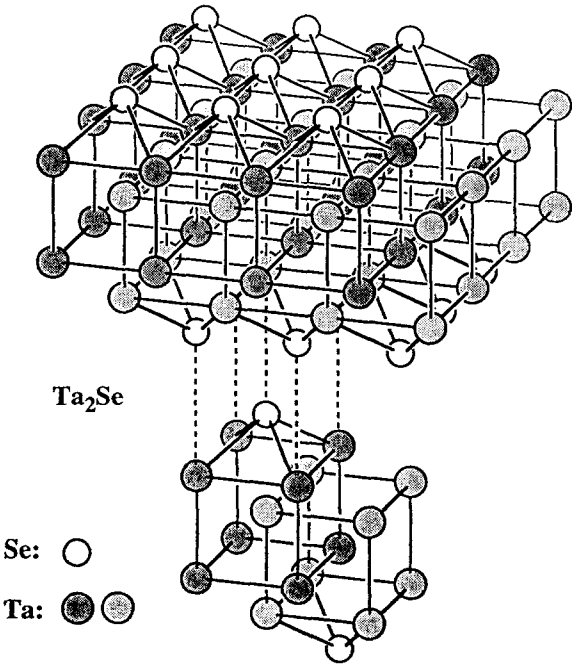

Fig. 1. The layered structure of Ta_2Se. The relationship to the b.c.c. structure is emphasized by differences in shading of the Ta centers. Dashed lines indicate long Ta–Se contacts between layers.

attribute this segregation to the differential in metal–metal bond strengths—since these bond strengths should decline in the order Ta–Ta > Ta–Nb > Nb–Nb, a structure with surrounds Ta with the greatest number of metal neighbours should be the most stable. The layered structure is a natural choice if the differential in M–S bond strengths is smaller than the metal–metal bond strengths. Franzen's group has also found that a five-layered material with the composition $Nb_{1.72}Ta_{3.28}S_2$ could be synthesized under special conditions and the same segregation of Nb into the exterior metal layers of the slab was observed [16].

Quite recently, we discovered a new material in the Hf–Te system, Hf_3Te_2, which a three-layered analog of Ta_2Se. In a fashion similar to Ta_2Se, Hf_3Te_2 has layered structure in which slabs are made up from three square nets of Hf sandwiched between two layers of Te. These Te–Hf_3–Te sandwiches are stacked, with very weak interlayer interactions, to form the full three-dimensional (3D) structure (Fig. 2). Each of the outer Hf metal atoms makes four bonds to the Hf atoms in the central net (3.1229(4) Å) and one longer bond through the slab (3.4454(12) Å) to a symmetry equivalent atom. Each Te is five coordinate with respect to Hf atoms in the same slab (Tel–Hf2, $4 \times 2.9120(5)$; Tel–Hf1, $1 \times 3.0245(9)$ Å). This compound came as a surprise to us since the valence electron concentration (the number of electrons available for metal–metal bonding) is much lower than that of the Ta compounds already dis-

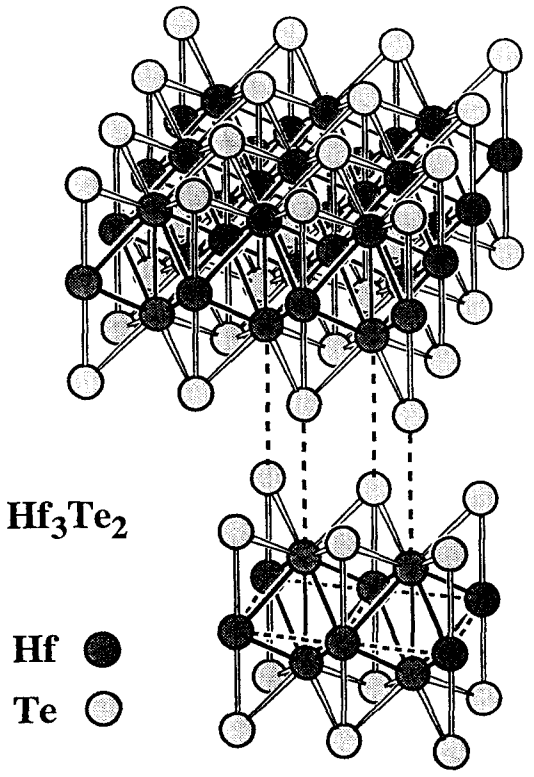

Fig. 2. The layered structure of Hf_3Te_2. The Hf–Hf distances that are short enough for appreciable bonding are indicated with full lines. Hf–Hf distances between atoms in the same layer are rather long (3.684 Å) and are indicated with dashed lines.

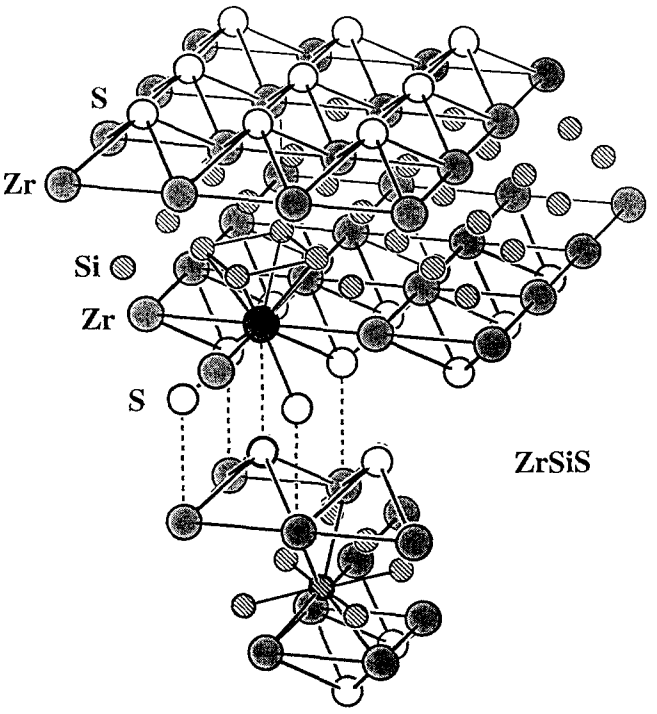

Fig. 3. A schematic diagram of the layered structure of ZrSiS. The environment of darkened atoms is drawn in the most detail. Note that interactions between layers (dashed lines) are essentially the same as in Ta_2Se and Hf_3Te_2.

cussed. Also, isoelectronic Zr_3Te_2 adopts a defect-WC structure as do the other known Group IV chalcogenides of the same composition [17–19].

The compounds discussed above belong to a broader class of chalcogenides based on stacking of 4^4 nets of atoms. There is a transition from 3D to 2D structures in these materials that seems to be determined by the *a* dimension and the size of the chalcogenide. Three additional layered tellurides, ZrZTe (Z ≡ Si, Ge, Sn), are useful to compare with these compounds in order to illustrate this 2D vs. 3D dichotomy. ZrSiTe has a layered structure built from square nets to form slabs with an internal stacking sequence Te–Zr–Si_2–Zr–Te (Fig. 3) [20,21]. ZrSiTe and ZrGeTe have been known for some time, though only for the former has a single-crystal structure determination been performed and that was quite recent [21,22]. ZrSnTe is a new member of this series and was only synthesized recently in our laboratory [22]. The internal structures of Hf_3Te_2 and ZrSiTe are somewhat different; Hf_3Te_2 has a central layer of Hf that is packed in the *ab*-plane at the same number density as the two adjacent metal layers, while the central Si layer in ZrSiTe-type forms a square net that is rotated by 45° and has a number density that is twice the atomic number density of the two adjacent Zr layers. The reader will also notice that the two outer metal layers within the Hf_3Te_2 slabs are stacked directly on each other while the two Zr layers are displaced in the *ab*-plane by (1/2, 1/2, 0). Despite these differences, the pairwise interactions *between* layers in the ZrZTe series are the same as those seen for Ta_2Se, $Ta_{1.4}Nb_{0.6}S$, and Hf_3Te_2. Table 1 shows some key structural parameters that aid in the comparison of these interlayer interactions.

As we move along the series of compounds

Table 1
Interatomic distances (Å) in several metal-rich layered chalcogenides[a]

$Ta_{1.4}Nb_{0.6}S_2$	Ta(Nb)–S^i	4 × 2.54	S^i–S^o	3.23
		1 × 2.67	Ta(Nb)–S^o	3.13
Ta_2Se	Ta–Se^i	4 × 2.67	Se^i–Se^o	3.55
		1 × 2.84	Ta–Se^o	3.82
Hf_3Te_2	Hf–Te^i	4 × 2.96	Te^i–Te^o	3.89
		1 × 3.13	Hf–Te^o	4.19
ZrSiTe	Zr–Te^i	4 × 2.92	Te^i–Te^o	3.73
			Zr–Te^o	3.96
ZrGeTe[b]	Zr–Te^i	4 × 2.93	Te^i–Te^o	3.51
			Zr–Te^o	3.26
ZrSnTe	Zr–Te^i	4 × 3.04	Te^i–Te^o	3.54
			Zr–Te^o	3.09

[a] Bonds to S^i, Se^i, and Te^i are within a layer; bonds to S^o, Se^o, and Te^o are between layers; S^i–S^o, Se^i–Se^o, and Te^i–Te^o are nonbonded contacts between layers.
[b] Values listed for ZrGeTe are estimates.

$Ta_{1.4}Nb_{0.6}S \rightarrow Ta_2Se \rightarrow Hf_3Te_2$, the distances between chalcogens in adjacent layers increase smoothly (3.23 → 3.55 → 3.89 Å) by an amount consistent with the increasing van der Waals radii. In contrast, the interatomic distances between metal centers and chalcogens on adjacent layers increase much more rapidly (3.13 → 3.82 → 4.19 Å), the import of which can be understood by comparison with the mean metal–chalcogen bond lengths within the layers (2.57 → 2.70 → 2.99 Å). Because the metal and chalcogen identity remain the same in the ZrZTe series, comparisons are made even more simply. (Distances for the Ge compound are estimates based on lattice parameters and structural constraints; no single-crystal structural investigation has been performed.) As we move along the series ZrSiTe → ZrGeTe → ZrSnTe, Te–Te distances between layers decline (3.73 → (3.55) → 3.54 Å) while interlayer Zr–Te distances decline dramatically (3.96 → (3.26) → 3.09 Å). At the same time, Zr–Te bond lengths within the layers expand some (2.92 → (2.93) → 3.04 Å). All of these data indicate that there is a rather abrupt, sterically controlled, crossover between compounds that are essentially 2D and 3D. In the ZrZTe series, bond length constraints on the central Z_2 square-net determine the spacing of the Zr and Te centers in the rest of the slab. When the Te–Te spacing in the slab is sufficiently large, steric crowding between Te atoms is lessened enough to permit the formation of interlayer Zr–Te bonds. The same crossover occurs in the new metal-rich materials. For Hf_3Te_2, the average Hf–Te bond length within the layer is bracketed by the distance for Zr–Te bonds in the ZrZTe series. The Hf–Te interlayer distance is 40% longer than the Hf–Te bonds; a similar ratio of distances holds for Ta_2Se. In $Ta_{1.4}Nb_{0.6}S$, the interlayer Ta(Nb)–S distance is only 22% longer and some weak interlayer bonding is implicated. Of the six compounds discussed, Hf_3Te_2, Ta_2Se and ZrSiTe are quite 2D and are promising candidates for intercalation chemistry, if the activation barrier involved in initiating the intercalculation reaction can be overcome.

2.2. Interstitially stabilized compounds

The strong bonding that occurs between early- and late-transition metals has been known for quite some time [23–26] but only recently have such "polar-intermetallic" bonds been incorporated intentionally into ternary metal-rich compounds as part of a synthetic strategy. The Zr and rare-earth cluster halide compounds discussed by Corbett in another paper in this volume (and below) stand as particularly conspicuous examples where late-transition metals can be viewed as "interstitials" encapsulated by early metal polyhedra (usually octahedra) within ternary phases. Thus, $Zr_6Cl_{14}Fe$ is a compound in which Fe occupies the center of a Zr octahedral cluster and participates in six short Zr–Fe bonds (average 2.43 Å) [27]. The strength of the intermetallic bonding is indeed underscored by emphasizing that this thermodynamically stable compound does not possess any Fe–Cl bonds, certainly a counterintuitive result to many inorganic chemists! Such is also the case in the many metal-rich halides of Zr and the rare-earths that are now known wherein late transition metals are so encapsulated [28–37].

Harbrecht discovered a class of Ta and Nb chalcogenides in which Fe, Co and Ni are encapsulated within tricapped trigonal prisms (tetrakaidecahedra) of the group five metal [38,42]. The series of compounds $Ta_9M_2S_6$ (M ≡ Fe, Co, Ni) was the first representative of this class of materials (Fig. 4) [38,39]. The environment of the "interstitial" transition metals is similar to what one finds in the Zr-rich binary intermetallic Zr_3Fe, and the numbers of electrons available for Fe–Ta and Fe–Zr bonding in $Ta_9Fe_2S_6$ and Zr_3Fe are similar (after accounting for the effective oxidation of the metal-metal bonding network by sulfur in the ternary compound). A striking feature of the $Ta_9Fe_2S_6$ structure is the presence of channels and the general segregation of metals and non-metals into separate structural domains. It is as if these just are cluster compounds where the metal atoms happen to outnumber the non-metals. Other compounds uncovered by Harbrecht of this general type include $Ta_{11}M_2Se_8$ (M ≡ Fe, Co, Ni) [40] and Ta_8NiSe_8 [42].

We have explored the Zr chalcogenide systems for signs of chemistry that is similar to the ternary intermetallic chemistry reported by Harbrecht and have so far found no sign of any analogs. Hf, however, has yielded some new materials in this area. A set of compounds with the composition Hf_8MTe_6 (M ≡ Mn,

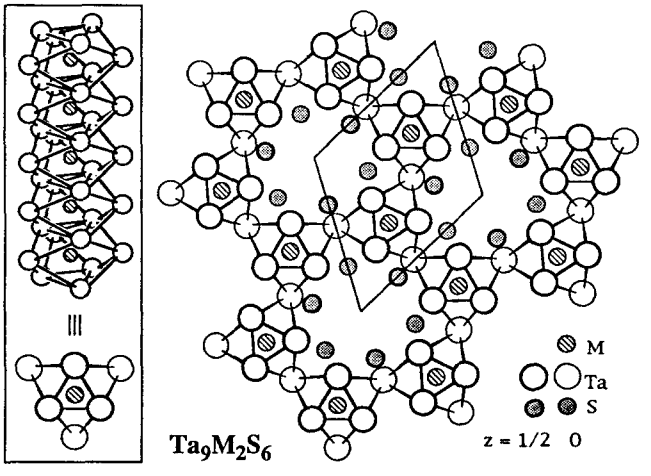

Fig. 4. The structure of $Ta_9M_2S_6$ compounds, with emphasis placed on the Ta polyhedra. The boxed illustration at left shows the chains shown in projection at right.

Fe, Co, Ni, Ru) adopts the structure depicted in Fig. 5, projected onto the *ac* plane. The Hf_8MTe_6 structure can be well described as an intergrowth of distorted M-centered tetrakaidecahedral Hf clusters and edge-sharing Hf telluride chains. The Te atoms serve to sheath the 3D metal framework and produce large cavities within the structure. In this depiction only the metal–metal bonding framework is shown. The chains of M-centered clusters in the Hf_8Te_6M structure are built up from Hf_3 triangles stacked along the *b*-axis to form infinite chains of trigonal prisms. Each of the three square faces of these prisms is capped by another Hf atom. At the center of each trigonal prism sits an M atom. The columns are linked by bonds between an Hf atom of each inner trigonal prism and a capping Hf of a neighboring chain's cluster, yielding a 2D layer that propagates in the *bc* plane. The unit cell contains two such layers running in opposite directions and stacked along the *a*-axis. The portion of the structure connecting these slabs is closely related to a portion of the Hf_3Te_4 structure (Nb_3Te_4-type) [43].

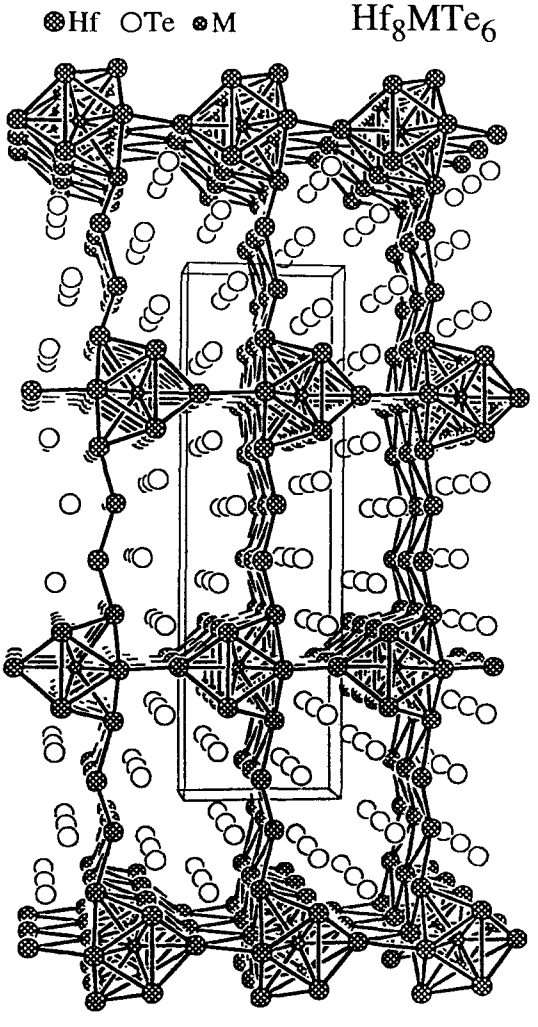

Fig. 5. A view of the structure of Hf_8MnTe_6. The chains of tricapped trigonal prisms that form the building blocks of this structure are evident. Only bonds between metal atoms are indicated.

In Hf_8MnTe_6, the Hf_6Mn trigonal prisms which form the inner cluster core are shaped such that the short Hf–Hf contacts are all in the triangular faces. These faces are distorted in an isosceles fashion forming one long (3.565 Å) and two short (3.160 Å) Hf–Hf contacts. The triangles are separated from each other by the *b*-axis dimension, 3.761 Å. This is much longer than the corresponding Ta–Ta distances in the structurally related compounds discussed above. Distances within the M-clusters of Hf_8Te_6Mn and Ta_8Se_8Ni are compared in **1**. The most significant difference between the clusters is the distortion of the triangular faces of Hf_8Te_6Mn. The shortest distances between triangular faces occurs in the related sulfide $Ta_9S_6Fe_2$ (3.297 Å). This distance in the related selenides is somewhat longer (about 3.45 Å). In Hf_8Te_6Mn, short Hf–Hf distances between triangular faces are excluded by the packing requirements of the Te atoms, and the lower metal-based electron concentration in the Hf compounds is consistent with this feature.

Very recent results indicate that compounds with the composition $Hf_{10}M_2Te_6$ (M ≡ Fe, Co) can also be prepared and similar double are built up from similar double chains of tricapped trigonal prisms [44].

It is clear that strong early–late intermetallic bonding motifs can be successfully incorporated into ternary chalcogenides as a central feature. However, in this chemistry, as in much of the metal-rich chemistry discussed, the differences between second- and third-row transition metal systems remain largely mysterious. We do not understand why Hf seems so much more inclined than Zr to form the ternary chalcogenides just discussed. Indeed, the situation for the halides seems to be the reverse: it is Zr that has the richer cluster chemistry [45]. By the same token, it is not clear why binary metal-rich chalcogenides of niobium and tantalum display as many differences as they do, even after accounting for the differential in metal–metal bond strengths. Of course, such mysteries

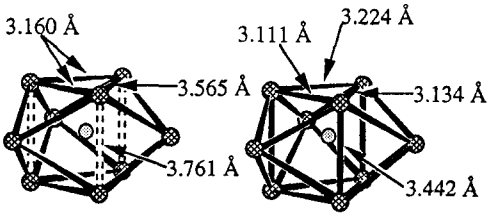

1

are sure to make synthetic exploration all the more rewarding for the surprises which continually appear.

3. Low-dimensional metals as precursors; cluster excision

In much of the above, we have described the results of synthetic exploration of metal-rich systems. If chemistry is to continue to progress fundamentally, and if fresh ideas are to flow continually into the field, such work must be sustained in the future. Nevertheless, we must at the same time investigate the properties and potential reactivity of these newly synthesized materials. In the absence of such investigations, there is the danger that synthesis and structural characterization becomes an exercise in "butterfly collecting" and that fruits of synthetic efforts will be unexploited for their potentially interesting and useful properties.

In one effort to extend metal-rich solid state chemistry beyond its traditional domain, we and others [46–48] have had an interest in using a wide range of metal-rich solids as a rich source of metal–metal bonded molecules (clusters) and polymers (chains) for solution chemistry. If metal–metal bonded species can be extracted successfully from solids, certain advantages apply. Not least of these advantages is the fact that many solid-state cluster (and condensed cluster) phases are thermodynamically stable and can therefore be prepared in high yields, nearly free from impurities. As a practical matter, it also turns out that many cluster-containing phases are the only compounds known in which their constituent clusters have been found.

The use of solid state precursors for cluster chemistry has a long history. Indeed, many methods for obtaining the six-metal cluster core species $Mo_6Cl_8^{4+}$ [49–53] and $(Nb, Ta)_6Cl_{12}^{n+}$ [54–60] relied on excising them from solid state precursor phases. Similarly, the trinuclear cluster $Re_3Cl_{12}^{3-}$ can be obtained from the solid $ReCl_3$ (equivalent to $[Re_3Cl_6]Cl_{6/2}$) [61–64].

The solid-state chemistry of Zr clusters is astoundingly variable yet synthetically controllable. Among the halides (X ≡ Cl, Br, I), only one basic cluster type is known; this is a cluster with a centered octahedral core ($(Zr_6Z)X_{12}$, depicted in Fig. 6). The most significant source of diversity in this chemistry lies in the range of centering atoms (Z) that have been found capable of filling the cluster. A listing of these interstitials follows, along with some $(Zr_6Z)X_{12}$-based compounds serving examples for the interstitials:

H $Zr_6Cl_{12}H$ [68], $Li_6Zr_6Cl_{18}H$ [65]

Be $Zr_6Cl_{12}Be$, $KZr_6Br_{13}Be$, $(Na, Cs)_4Zr_6Cl_{16}Be$ [66–68], $K_3Zr_6Cl_{15}Be$ [69]

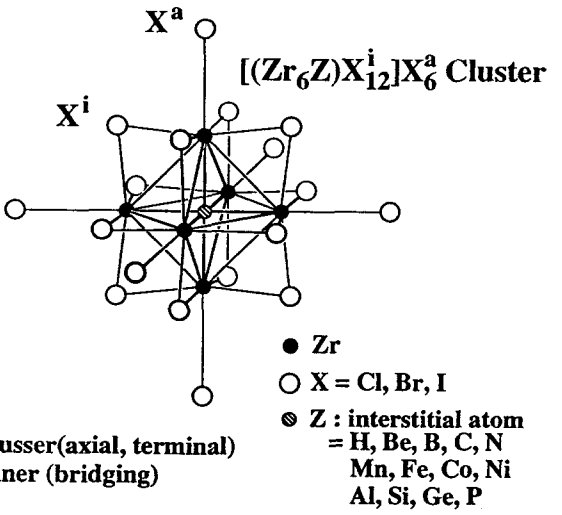

Fig. 6. The basic $[(Zr_6Z)X_{12}]X_6$ cluster. The "inner, ausser" notation is illustrated.

B $Zr_6Br_{12}B$, $Zr_6Cl_{13}B$, $Zr_6Cl_{14}B$, (Cs–Na) $Zr_6Cl_{14}B$, $(Na, K)_2Zr_6Cl_{15}B$, $CsKZr_6Cl_{15}B$ [66, 70, 77], $Zr_6I_{12}B$ (K, Cs)$Zr_6I_{14}B$ [72], $Cs_3Zr_6Cl_{16}B$ [67], $Rb_5Zr_6Cl_{18}B$ [73]

C $Zr_6Cl_{14}C$, (Cs, Rb, K)$Zr_6Cl_{15}C$ [66], $Zr_6I_{12}C$, $Zr_6I_{14}C$, (K, Rb, Cs)$Zr_6I_{14}C$ [74], $Cs_3Zr_6Cl_{16}C$ [67], $Rb_4Zr_6Cl_{18}C$ [65]

N $Zr_6Cl_{15}N$ [71]

Al $Cs_{0.7}Zr_6I_{14}Al$ [72]

Si $Cs_{0.3}Zr_6I_{14}Si$ [72], $Zr_6I_{14}Si$ [75]

P $Zr_6I_{14}P$, $(Cs, Rb)_xZr_6I_{14}P$ [75]

Mn $CsZr_6I_{14}Mn$, $Zr_6I_{12}Mn$ [28,29], $Li_2Zr_6Cl_{15}Mn$ [76]

Fe $Cs_{0.63}Zr_6I_{14}Fe$, $Zr_6I_{14}Fe$ [28,29], $LiZr_6Cl_{15}Fe$ [76]

Co $Cs_xZr_6I_{14}Co$ [28,29], $Zr_6Cl_{15}Co$ [76]

Ni $Zr_6Cl_{15}Ni$ [76]

Some compounds have been grouped together because they are stoichiometrically related, even if they do not have the same structure, for example the cluster connectivity in $KZr_6Cl_{15}C$ is different from that of the (Rb, Cs)$Zr_6Cl_{15}C$ pair of compounds.

A problem that surfaced early in attempts to excise Zr-clusters from solids was the observed oxidation of certain clusters and uncertainty about the identity of the oxidant involved [77,78]. Thus, Rogel and Corbett isolated $(Et_4N)_4Zr_6Cl_{18}Be \cdot 2CH_3CN$ from the solid-state precursor $K_3Zr_6Cl_{15}Be$, indicating a net two-electron oxidation of the Be-centered clusters on dissolution. Similarly, these workers isolated $(Et_4P)_4Zr_6Cl_{18}B \cdot (Et_4P)_2ZrCl_6$, containing the $13e^-$ cluster $[(Zr_6B)Cl_{18}]^{4-}$ and the $ZrCl_6^{2-}$ ion, from the precursor solid $Rb_5Zr_6Cl_{18}Br$, a $14e^-$ cluster compound. In both cases, the oxidant(s) were not identified. However, the highly charged clusters $[(Zr_6B)Cl_{18}]^{5-}$ and $[(Zr_6Be)Cl_{18}]^{6-}$ should be strong-

ly reducing and the possibility that the solvent (CH_3CN) had been reduced was suggested [77].

There exists a rather unique solvent system that we have found to be useful for the dissolution of Zr halide cluster compounds. The room-temperature melts ImCl–$AlCl_3$ (**2**, Im ≡ 1-methyl-3-ethylimidizolium) can effectively dissolve all those compounds that are known to be readily soluble in acetonitrile and several that are not.

This solvent system [79–83] has been, and will continue to be, useful for several reasons. (a) Most obviously, the melt is liquid at ambient temperature [84,85]. This makes handling convenient, and allows us to do chemistry at temperatures where the clusters' reactivity is lower and the likelihood that glass containers will be attacked is virtually nil. (b) Like acetonitrile, this solvent allows a good spectroscopic window for the study of electronic spectra (at ambient temperature). For example, the spectrum of $[(Zr_6Fe)Cl_{12}Cl_6^a]^{4-}$ cluster is virtually identical in ImCl–$AlCl_3$ and acetonitrile from the near IR region to 36 000 cm^{-1} in the UV. The ImCl–$AlCl_3$ liquid system has the additional characteristic that it may eliminate the enhanced solvation effects that are often observed for polar solvents such as CH_3CN and $(CH_3)_2SO$ [86]. (c) There seems to be less sensitivity of ImCl–$AlCl_3$ melts to reduction by the some of the strongly reducing $(Zr_6Z)Cl_{12}^{n+}$ clusters [86–89], for example the $(Zr_6Be)Cl_{12}$ cluster has a noticeably greater stability in ImCl–$AlCl_3$ solutions. The usefulness of these ionic liquids for the electrochemical study of several well known inorganic cluster systems has been demonstrated; these include $[Mo_2Cl_8]^{4-}$ [90], $[(Mo_6Cl_8]Cl_6]^{2-}$ [91], $[Re_2Cl_8]^{2-}$ [88], $[Re_2Cl_8]^{3-}$ [92], $[Re_3Cl_{12}]^{3-}$ [88], $[W_2Cl_9]^{3-}$, and $[(Nb_6Cl_{12})Cl_6]^{n-}$ [93].

When clusters are to be excised from a solid phase, Lewis bases are necessary to fill exo coordination sites on the cluster which are occupied by intercluster halide bridges in the solid state. For this reason, successful cluster excision occurs for an ImCl–$AlCl_3$ melt rich in the organic salt ($ImCl:AlCl_3 \approx 7:3$); the excess of Cl^- over $AlCl_3$ makes the melt basic in the Lewis sense. Conventional M^1Cl–$AlCl_3$ melts (M^1 ≡ alkali metal) are not suited for cluster excision at low temperatures, because although some have reasonably low eutectic temperatures (around 100–150°C), the eutectic compositions are acidic ($M^1Cl:AlCl_3 < 1$). Under basic conditions ($M^1Cl:AlCl_3 > 1$), where cluster solubilities might be appreciable, the melting points are high. In short, ImCl–$AlCl_3$ molten salts are advantageous for cluster excision because they can be made basic while remaining in the liquid state.

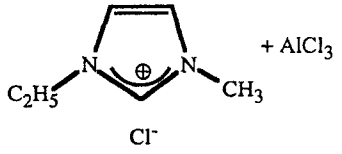

2 (ImCl/$AlCl_3$)

It has been generally observed that the most readily dissolved cluster-based compounds are those in which intercluster linkages are minimized [46]. Holm and coworkers report that they are able to excise intact $Re_6Se_5Cl_9^-$ and $Re_6Se_6Cl_8^{2-}$ clusters from the respective 1D $Re_6Se_5Cl_8$ and the 2D $Re_6Se_6Cl_6$, but that the 3D solid $Re_6Se_7Cl_4$ resists dissolution [47,48]. We were therefore surprised to discover that 3D linked compounds $Zr_6X_{14}Fe$ (see Fig. 7) are soluble in the ImCl–$AlCl_3$ ionic liquid. Deep blue and violet solutions are observed for the Fe-centered chloride and bromide clusters respectively, and we find that the UV–visible spectrum obtained for the $[(Zr_6Fe)Br_{12}Cl_6^a]^{4-}$ cluster closely resembles the spectrum we reported for the chloride cluster (see Fig. 8) [94]. The $Zr–X^{i-a}$ intercluster linkages found in these halide-poor solids are a necessity for a 6–12 cluster compound with a net halide: Zr ratio of less than 15:6 (see Fig. 7).

Other compounds that resist dissolution in CH_3CN at ambient temperature are cleanly dissolved into the ImCl–$AlCl_3$ melt. $Li_2Zr_6Cl_{15}Mn$ dissolves quickly into the melt at 160°C and when the solution so obtained is mixed with CH_3CN and then layered with Et_2O–hexane, $(Im)_5[(Zr_6Mn)Cl_{18}] \cdot 1.5CH_3CN$ crystallizes at the interface. The structure of the $[(Zr_6Mn)Cl_{18}]^{5-}$ cluster is comparable with the structure of the cluster in the starting material.

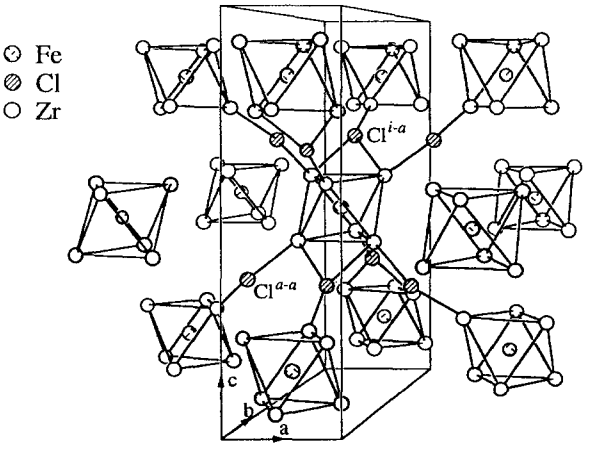

$Zr_6Cl_{14}Fe = [(Zr_6Fe)Cl_{10}^{i}Cl_{2/2}^{i-a}]Cl_{4/2}^{a-a}$ (Nb_6Cl_{14} type)

Fig. 7. Intercluster linkages are emphasized in this depiction of the common $(Zr_6Z)Cl_{14}$ structure type. Only halides that serve to bind the central cluster to its neighbors are indicated. The tight coupling provided by Cl^{i-a} linkages makes these compounds difficult to dissolve in conventional solvents.

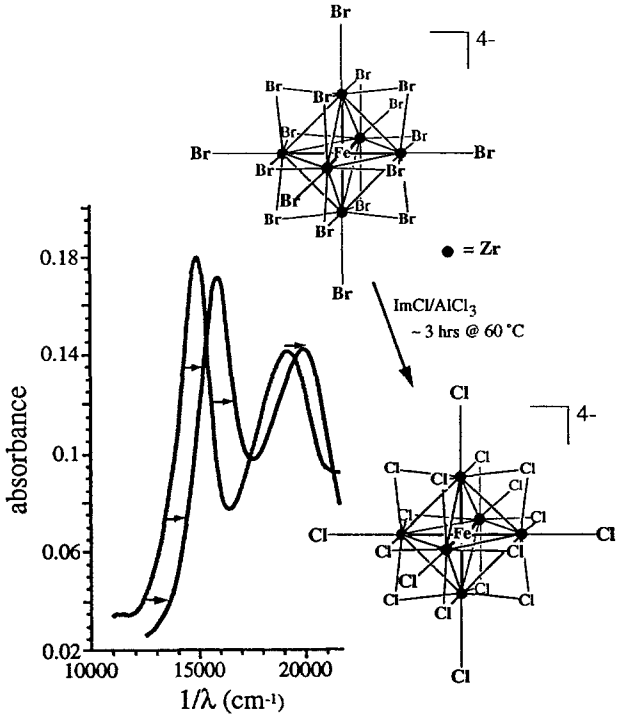

Fig. 8. The UV–visible spectral blue shift that accompanies bromide to chloride replacement is indicated. This shift is manifest as a violet to blue color change in the solution.

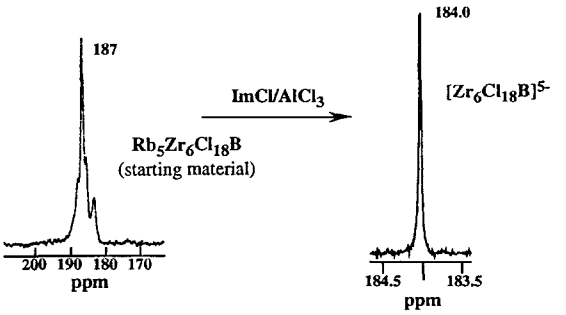

Fig. 9. Excision of clusters from solid state precursors can be followed by NMR for clusters encapsulating appropriate nuclei. The chemical shift and narrow line width of the ^{11}B signal are characteristic of a cluster centered by boron.

We have observed that ImCl–$AlCl_3$ melts enable the exchange of inner halides on the clusters (Fig. 8); such exchange occurs in hours at temperatures near 100°C and even at room temperature over a period of days [95]. This exchange reaction was first observed to accompany the excision of $[(Zr_6Fe)Br_{12}^{4+}]$ clusters from $Zr_6Br_{14}Fe$. The X-ray structure of the compound $[Im]_4[(Zr_6Fe)Cl_{18}]$, resulting from the excision of clusters from $Zr_6Br_{14}Fe$ in an ImCl–$AlCl_3$ melt, shows that both ausser and inner bromides (Br^a and Br^i) are displaced by chlorides from the melt.

After a means of dissolving cluster compounds without cluster decomposition is devised, the identity of the product is confirmed with the least ambiguity by isolating crystals of a cluster-containing product and determining the crystal structure. Despite this, other spectroscopic information is necessary if one hopes to understand the chemistry occurring in the dissolution process and reactions conducted in solution (intentionally or not). The NMR characteristics of some interstitials allow one to monitor the dissolution of these cluster compounds in a fairly direct manner. Fig. 9 below shows one solid-state and one solution ^{11}B NMR spectrum. A solid-state MAS spectrum for the precursor $Rb_5Zr_6Cl_{18}B$ is shown an the left, and a solution spectrum taken after dissolving $Rb_5Zr_6Cl_{18}B$ in a basic $AlCl_3$–ImCl ionic liquid appears on the right. The chemical shifts observed in each case are quite similar and strongly indicative of B encapsulated within a metal $[(Zr_6B)Cl_{18}]^{5-}$ cluster [96–101]. The very narrow line width (2.3 Hz) for the spectrum taken in the $AlCl_3$–ImCl ionic liquid is consistent with the symmetrical environment in which the quadrupolar ^{11}B nucleus sits, but broadens considerably in samples where incidental cluster oxidation has taken place. This is presumably due to accelerated relation of ^{11}B nuclei caused by contamination with paramagnetic $13e^-$ $[(Zr_6B)C_{18}]^{4-}$ clusters.

Hussey and coworkers' observations of the solubility behavior of the $[Mo_6Cl_8]^{4+}$ ion in ImCl–$AlCl_3$ melts indicates a generalized amphoterism that may be useful for using these melts as crystal growth media [91]. $MoCl_2$ (equivalent to $(Mo_6Cl_8^i)Cl_2^aCl_{4/2}^{a-a}$) has low solubility in a neutral (50:50) ImCl–$AlCl_3$ melt, but its solubility increases markedly in both basic and acidic melts. In basic melts, the cluster is clearly dissolved as the $[Mo_6Cl_{14}]^{2-}$ ion; in acidic melts it is likely that the cluster is solvated by $AlCl_4^-$ or $Al_2C_7^-$ ions:

$$\underset{\text{basic}}{[(MO_6Cl_8)Cl_6]^{2-}(l)} \xleftarrow{+ImCl} \underset{\text{neutral (ImCl: } AlCl_3=50:50)}{(Mo_6Cl_8)Cl_{4/2}^{a-a}Cl_2^a(s)}$$

$$\xrightarrow{+AlCl_3} \underset{\text{acidic}}{\text{“}[(Mo_6Cl_8)(AlCl_4)_6]^{2-}(l)\text{”}}$$

We have found that in ImCl–$AlCl_3$ melts, $[(Zr_6Z)Cl_{12}]^{(6-n)+}$ cluster cores experience significant perturbation when they are titrated from the basic to acidic regimes by addition of $AlCl_3$. It is likely that this is due to the formation of $[(Zr_6Z)Cl_{12}](AlCl_4)_6^{n-}$—UV–visible spectra are strongly blue shifted when compared with spectra observed for $[(Zr_6Z)Cl_{12}]Cl^{n-}$ clusters in the basic ionic liquid or in acetonitrile (Fig. 10). The magnitude of these spectral shifts is much larger than is observed when ausser chlorides are substituted by any number of other ligands we have examined (e.g. amines or phosphines) [94,102]. This is a simple consequence of

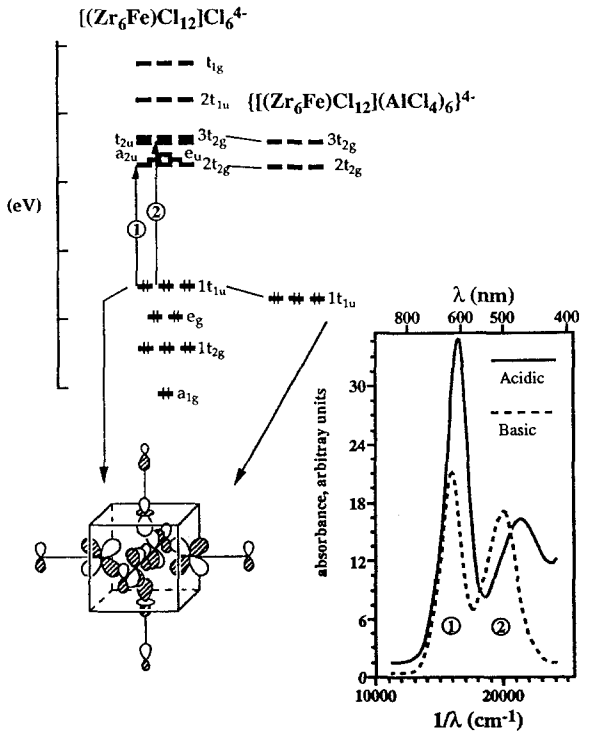

Fig. 10. The blue shift that occurs when the $[(Zr_6Fe)Cl_{12}^{2+}]$ cluster is titrated into acidic melts is illustrated. Molecular orbital calculations are consistent with the interpretation that this is due to binding by the very weak $AlCl_4^-$ donors.

the very low donor strength of the $AlCl_4^-$ ion and the orbital character of the cluster HOMO (Fig. 10).

We think the future for the use of ionic liquids for the investigation of metal clusters is bright. In fact, we are beginning to investigate whether metal–metal bonding chain compounds might not also be solubilized in ionic liquids. In many instances, the bonds which bind chains together in the solid state are of the same type as the bonds that cross-link clusters in compounds which we have already been able to dissolve. When one examines the broad range of metal-rich compounds in which we find low-dimensional metal–metal bonded arrays (clusters, chains, and layers), the incentive for developing means whereby we can carefully dismantle them is strengthened.

4. Bonding and properties [103–105]

An examination of the structures of the metal-rich compounds discussed above reveals that while many such compounds have low-dimensional structures insofar as their metal–metal bonded connectivity is concerned, they still possess unbroken and undistorted metal–metal bonded networks. This generates the strong impression that these materials will be metallic electrical conductors, at least along the direction(s) in which these networks propagate. While this assumption is usually correct, we now know several cases where compounds with extended metal–metal bonded networks are semiconductors. From a theoretical point of view, this means that there must be some formal way in which the delocalized band description of metal–metal bonding in the compounds can be transformed into a localized description in which electrons can be said to occupy bond orbitals in pairs. It does not mean that the localized description necessarily involves two-center—two-electron bonds; indeed, it is probably this fact that makes an intuitive recognition of a localized description more difficult than for Zintl (octet-rule) compounds.

4.1. Localization of metal–metal bonding electrons in MoS_2

MoS_2 and Y_2Cl_3 are two simple binary compounds which demonstrate how an extended metal–metal bonded network may exhibit localized metal–metal bonding. We first present, in some detail, how a localized metal–metal bonding scheme emerges within the layers of MoS_2 [103]. MoS_2 is a material build up by the fusion of MoS_6 trigonal prisms ($MoS_2 \equiv MoS_{6/3}$) into layers, which are in turn stacked (up the z axis) with van der Waals gaps between the layers. The semiconducting behavior of this d^2 compound has been traditionally explained by invoking a gap between the Mo d_{z^2} orbital (assigned to the valence band) and $\{d_{xy}, d_{x^2-y^2}\}$ orbitals (assigned to the conduction band). However, for the trigonal prisms such as they are found in MoS_2 and in most compounds where such trigonal prismatic coordination is manifest, the prism height-to-base ratio is such that the d_{z^2} orbital and $\{d_{xy}, d_{x^2-y^2}\}$ orbitals are nearly degenerate. This means that the band gap cannot be explained by the local "crystal-field" splitting between d_{z^2} and $\{d_{xy}, d_{x^2-y^2}\}$. It also means that we can freely take linear combinations of these three d orbitals for purposes of examining any Mo–Mo bonding effects, if such combinations better illuminate the nature of the metal–metal bonding.

As it turns out, the localized valence and conduction band orbitals of MoS_2-like layers (including MCh_2 ($M \equiv$ Mo, Ta, Nb; $Ch \equiv$ S, Se), LnX_2 ($X \equiv$ halides), and $LiNbO_2$) are easily understood if we start with three equivalent "hybrid" orbitals constructed as linear combination of the d_{z^2} and $\{d_{xy}, d_{x^2-y^2}\}$ orbitals:

$$\sigma_1 = \frac{-1}{\sqrt{3}} d_{z^2} + \sqrt{\frac{2}{3}} d_{x^2-y^2}$$

$$\sigma_2 = \frac{-1}{\sqrt{3}} d_{z^2} - \frac{1}{\sqrt{6}} d_{x^2-y^2} - \frac{1}{\sqrt{2}} d_{xy} \quad (1)$$

$$\sigma_3 = \frac{-1}{\sqrt{3}} d_{z^2} - \frac{1}{\sqrt{6}} d_{x^2-y^2} + \frac{1}{\sqrt{2}} d_{xy}$$

These orbitals project into the square faces of the prism (depicted in **3**). With these orbitals we can understand how the metal–metal bonding in a trigonal prismatic layer can at once be fairly strong, extend over the infinite 2D layer, and yet involve localization of the d electrons which is consistent with a semiconducting state. Each MoS_6 trigonal prism is imbedded within a layer and fused to six adjacent prisms in the manner illustrated in Fig. 11. The square faces of each MoS_6 prism abut the faces of empty S_6 prisms, the center of which also lies at the center of an Mo_3 triangle. Every such Mo_3 triangle in the layer has three hybrids of the type just discussed that extend toward its center from the Mo atoms at the vertices. Thus, each such Mo_3 triangle forms a three-center bonding system—two d electrons per Mo center reside in each of the three-center—two-electron bond orbitals.

The scheme **3** is more than just a schematic description of the metal–metal bonding in MoS_2-like layers. We have constructed Wannier orbitals from the valence and conduction band wavefunctions that yield local bond orbitals which can be considered as fully representative of the band orbitals from which they arise (i.e. the electron density obtained from the set of Wannier orbitals for a given band is exactly the same as the full set of band orbitals for the same band). These are plotted for the (MoS_2-like) PrI_2 layer in Fig. 12. Clearly, the valence band has three-center bonding character and the pair of local orbitals for the two overlapping conduction bands is just the two antibonding orbitals in the three-center system. When the layer has the proper electron count (two per metal center, or rather, two per three-center bond), the system is a semiconductor.

We have presented a few details concerning localized bonding in MoS_2-like systems because there are features which are general and are worth emphasizing. (a) The issue of whether an extended metal–metal bonded system is a metallic (electronic) conductor is distinct from the issue of whether the metal–metal bonding is strong or weak. The band gap in an MoS_2-like layered compound may actually be larger if the metal–metal bonding is stronger because the mean valence–conduction band splitting arises from the splitting between the bonding and antibonding orbitals in the three-center system. In $LiNbO_2$, the Nb–Nb distances (2.90 Å) are comparable with elemental Nb, but the compound is still semiconducting with an appreciable band gap. (b) In systems where metal–metal bonding is significant and forms an extended network, a semiconducting state will still prevail if the structure allows for sufficient spatial localization of electron pairs. If the words "metal–metal" were replaced by the word "covalent" in this statement, most chemists would regard it as obvious. Two problems

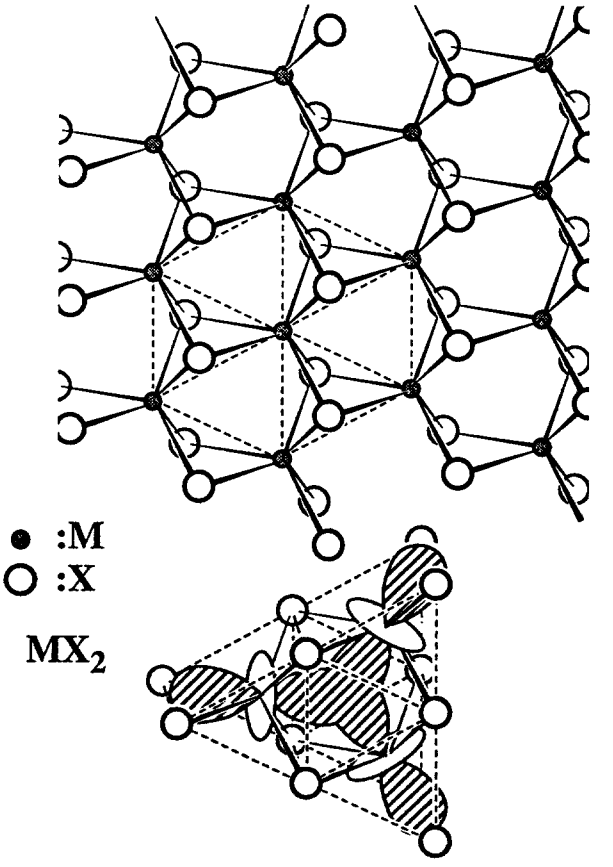

Fig. 11. One MX_2 layer is illustrated for metals with trigonal-prismatic coordination. The geometrical situation involved in the formation of three-center–two-electron bonds in such MoS_2-like compounds is depicted at bottom.

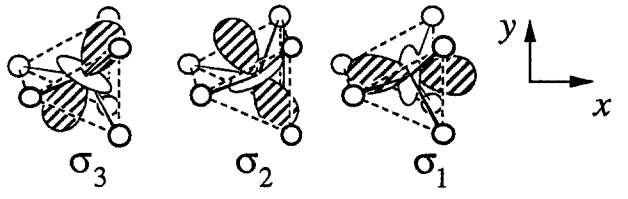

3

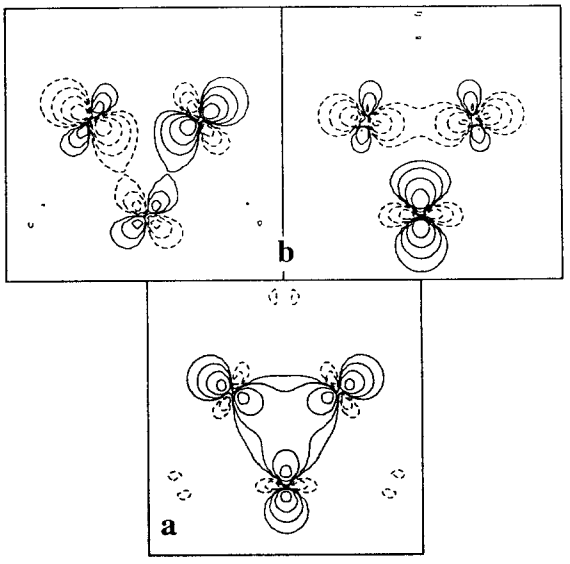

Fig. 12. Contour plots for local orbitals derived from the valence and conduction bands of the MoS_2-like layered material, PrI_2, are shown. The valence band 3c bonding orbital is shown at bottom in a; the two antibonding counterparts derived from the conduction band are plotted at top in b.

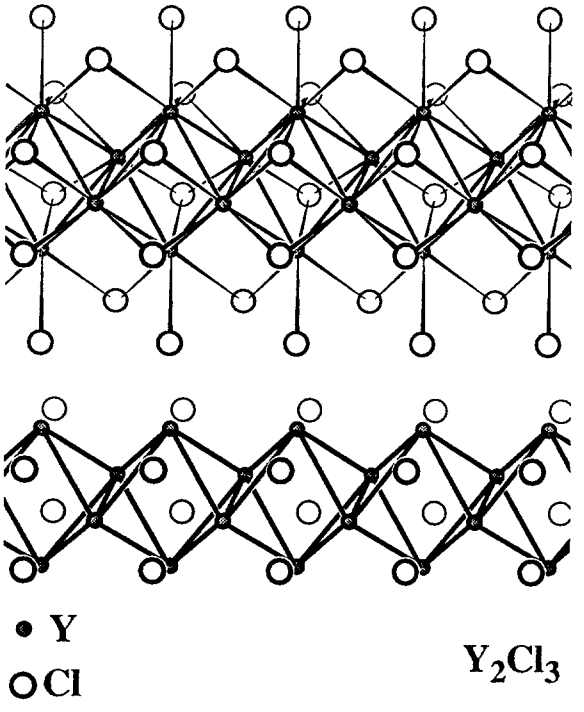

Fig. 13. Chains imbedded in the structure of Y_2Cl_3 are illustrated. At top, both Y–Y and Y–Cl linkages are shown. At bottom, Y–Y contacts are indicated with heavy lines.

remain, however. The first is the lingering idea that metal–metal bonding is somehow cleanly distinct from covalent bonding. It is not. There is no compelling reason to maintain the concept of the "metallic bond" as distinct from the "covalent bond". The second problem is that it remains difficult to recognize intuitively the circumstances under which "the structure allows for sufficient spatial localization of electron pairs". A few more examples will serve to illustrate this difficulty.

4.2. Localization of metal–metal bonding electrons in other systems

Y_2Cl_3 possesses an extended 1D chain structure in which the Y–Y bonded framework is often described as the result of condensation of octahedral clusters at opposite edges to form a linear chain (Fig. 13) [106]. The Y–Y bonded contacts short enough to imply significant bonding are those between Y atoms at the shared edges (3.27 Å) and between apical and basal Y centers (3.65 Å); these bonds are indicated at bottom in Fig. 13. The Y–Y contacts parallel to the chain propagation axis are too long (3.83 Å) to be consistent with such bonding—the "octahedra" are then useful only in a rough description of the structural connectivity and do not describe the "location" of the bonds. Y_2Cl_3-type compounds (analogs exist for Gd [107] and other lanthanides) are all semiconductors; the band gap for Gd_2Cl_3 is 0.85 eV [108]. Band structure calculations yield a very good estimate of this band gap; the calculations show that the Y 4d bands split such that three narrow overlapping bands lie isolated below the remainder of the 4d bands to accommodate the six d electrons available for metal–metal bonding per Y_4Cl_6 unit. Three well localized orbitals per unit cell, constructed from the wavefunctions for the three low-lying 4d bands, illuminate the structural origin of this compound's semiconducting properties [104]. One of the local orbitals indicates the presence of a two-center–two-electron bond between Y centers that form the junction of the distorted octahedra; the other two orbitals are four-center–two-electron "molecular orbitals" that spread across rhombuses as indicated in Fig. 14.

Especially important for understanding the nonmetallic state that holds for both Y_2Cl_3-type and MoS_2-type compounds is the near mutual ortogonality of the set of local orbitals for the valence and conduction bands. Not only are the local orbitals orthogonal to other local orbitals situated in the same unit cell, they have very little overlap with orbitals localized in adjacent cells. This is the reason that the valence and conduction bands do not "spread in energy" to close the band gap. This is fundamentally the same reason that any saturated organic polymer, such as polyethylene, is an insulator; the localized C–C bonds have an insufficient mutual overlap to close the gap between the σ and σ^* bands.

Challenges to our understanding of some "surprising semiconductors" have not yet been met. Metal–

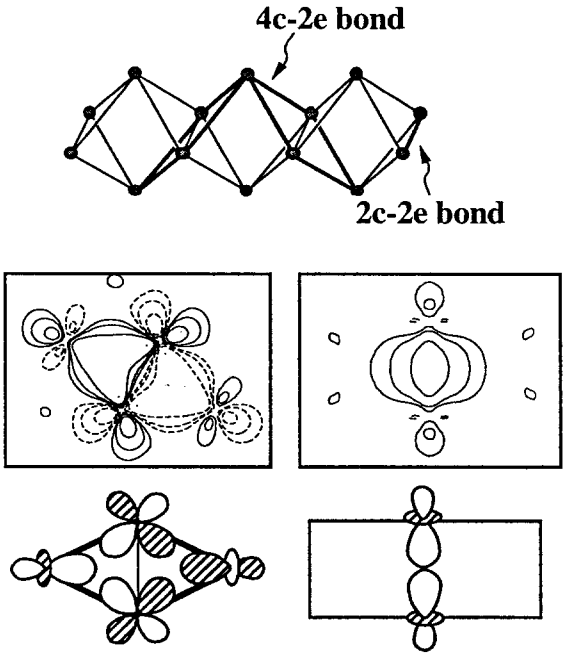

Fig. 14. The three local orbitals responsible for Y–Y bonding in Y_2Cl_3 are illustrated. Two identical four-center–two-electron bonding orbitals like that plotted at left spread over the bonds are indicated at top. A simple two-center–two-electron bond connects the two atoms at the junction of the edge-fused Y_6 octahedra.

metal bonds make up the central structural backbone of the chains found in the R_4Br_4Os ($R \equiv Y, Er$) compounds (Fig. 15) synthesized in Corbett's laboratories [34]. Measurements conducted in our laboratories

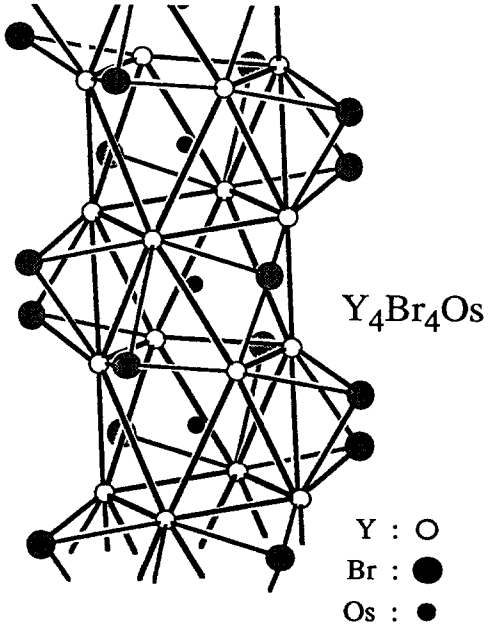

Fig. 15. A chain of Os-centered, fused square antiprisms that forms the basis for the structure of Y_4Br_4Os. Br atoms bind to external triangular faces of this Y_4Os chain and also bind to neighboring chains in a manner not shown.

reveal that these compounds are small-gap (0.16 eV) semiconductors [109]. This behavior is nicely consistent with the calculated band structure for Y_4Br_4Os using the extended Hückel method, in which a calculated valence–conduction band gap of 0.18 eV is found. Despite this satisfying computational agreement, the kind of structural understanding of the origins for the band gaps that we have extracted for MoS_2 and Y_2Cl_3 has not yet been attained for this system. How do the electrons localize in this system? As it turns out, we know that some localized bond orbitals can be constructed. Unfortunately, that knowledge does not give us an efficient algorithm for doing so. It is precisely this kind of understanding which we hope to acquire in probing structure–property relationships as chemists. Finally, whether or not our abilities to grasp intuitively these structure–property relationships in metal-rich materials improves, examples such as these do show that the conceptual separation between the metallic and covalent bond is artificial and should be eliminated.

Acknowledgments

This research was generously supported by the National Science Foundation through grant DMR-9215890 and by the Robert A. Welch Foundation through grant A-1132. I am especially indebted to the students and postdoctoral associates at Texas A&M who have conducted the research discussed herein: Sung-Jin Kim, Kirakodu Nanjundaswamy, Marcus Bond, Kyeong-Ae Yee, Charles Runyan, Jr., Kyungsoo Ahn, Yunchao Tian, Robert Abdon, Chwanchin Wang, and Jerry Harris.

References

[1] B. Harbrecht, *Angew. Chem. Int. Ed. Eng., 28* (1989) 1660.
[2] S.-J. Kim, K.S. Nanjundaswamy and T. Hughbanks, *Inorg. Chem., 30* (1991) 159.
[3] H. Wada and M. Onoda, *Mater. Res. Bull., 24* (1989) 191.
[4] M. Conrad and B. Harbrecht, *J. Alloys Comp., 187* (1992) 181.
[5] R.L. Abdon and T. Hughbanks, *Angew. Chem. Int. Ed. Engl., 33* (1994) 2328.
[6] M. Conrad and B. Harbrecht, *IVth European Conf. on Solid State Chemistry, Dresden, 1992*, Gesellschaft Deutscher Chemiker, 1992.
[7] F.A. Cotton and G. Wilkinson, *Advanced Inorganic Chemistry*, Wiley, New York, 1988, 5th edn.
[8] N.N. Greenwood and A. Earnshaw, *Chemistry of the Elements*, Pergamon, New York, 1984.
[9] B.R. Conard, L.J. Norrby and H.F. Franzen, *Acta Crystallogr. B, 25* (1969) 1729.
[10] J.G. Smeggil, *J. Solid State Chem., 3* (1971) 248.
[11] A. Simon, *Angew. Chem. Intl. Ed. Engl., 20* (1981) 1.
[12] X. Yao and H.F. Franzen, *J. Alloys Comp., 182* (1992) 299.

[13] K.S. Nanjundaswamy and T. Hughbanks, *J. Solid State Chem.*, *98* (1992) 278.
[14] H.F. Franzen, T.A. Beineke and B.R. Conrad, *Acta Crystallogr. B*, *24* (1968) 412.
[15] H.F. Franzen and J.G. Smeggil, *Acta Crystallogr. B*, *25* (1969) 1736.
[16] X. Yao and H.F. Franzen, *J. Am. Chem. Soc.*, *113* (1991) 1426.
[17] H. Hahn, B. Harder, U. Mutschke and P. Ness, *Monatsh. Chem.*, *292* (1957) 82.
[18] H. Hahn and P. Ness, *Z. Anorg. Allg. Chem.*, *302* (1959) 39.
[19] H. Sodeck, H. Mikler and K.L. Komarek, *Monatsh. Chem.*, *110* (1979) 1.
[20] H. Onken, K. Vierheilig and H. Hahn, *Z. Anorg. Allg. Chem.*, *233* (1964) 267.
[21] W. Bensch and P. Dürichen, *Acta Crystallogr. C*, *50* (1994) 346.
[22] C.C. Wang and T. Hughbanks, *Inorg. Chem.*, submitted for publication.
[23] L. Brewer, *Science*, *161* (1968) 115.
[24] L. Brewer and P.R. Wengart, *Metall. Trans.*, *4* (1973) 2674.
[25] A.R. Miedema, R. Room and F.R. d. Boer, *J. Less Common Met.*, *41* (1975) 283.
[26] A.R. Miedema, P.F. Chatel and F.R. d. Boer, *Physica B*, *100* (1980) 1.
[27] J. Zhang and J.D. Corbett, *Inorg. Chem.*, *32* (1993) 1566.
[28] T. Hughbanks, G. Rosenthal and J.D. Corbett, *J. Am. Chem. Soc.*, *108* (1986) 8289.
[29] T. Hughbanks, G. Rosenthal and J.D. Corbett, *J. Am. Chem. Soc.*, *110* (1988) 1511.
[30] T. Hughbanks and J.D. Corbett, *Inorg. Chem.*, *27* (1988) 2022.
[31] T. Hughbanks and J.D. Corbett, *Inorg. Chem.*, *28* (1989) 631.
[32] M. Payne, P. Dorhout and J.D. Corbett, private communication.
[33] M.W. Payne, P.K. Dorhout, S.-J. Kim, T.R. Hughbanks and J.D. Corbett, *Inorg. Chem.*, *31* (1992) 1389.
[34] P.K. Dorhout and J.D. Corbett, *J. Am. Chem. Soc.*, *114* (1992) 1697.
[35] Y. Park and J. Corbett, *Inorg. Chem.*, *33* (1994) 1705.
[36] R. Llusar and J.D. Corbett, *Inorg. Chem.*, *33* (1994) 849.
[37] M. Ruck and A. Simon, *Z. Anorg. Allg. Chem.*, *619* (1993) 327.
[38] B. Harbrecht and H.F. Franzen, *J. Less-Common Met.*, *113* (1985) 349.
[39] B. Harbrecht, *J. Less-Common Met.*, *124* (1986) 125.
[40] B. Harbrecht, *J. Less-Common Met.*, *141* (1988) 59.
[41] B. Harbrecht, *Z. Kristallogr.*, *182* (1988) 118.
[42] M. Conrad and B. Harbrecht, *J. Allows Comp.*, *197* (1993) 57.
[43] C.C. Wang, R.L. Abdon, T. Hughbanks and J. Reibenspies, *J. Alloys Comp.*, *99* (1995) in press.
[44] R.L. Abdon and T. Hughbanks, *Inorg. Chem.*, to be submitted.
[45] R.-Y. Qui and J. Corbett, *Inorg. Chem.*, *33* (1994) 5727.
[46] S.C. Lee and R.H. Holm, *Angew. Chem. Int. Ed. Eng.*, *29* (1990) 840.
[47] O.M. Yaghi, M.J. Scott and R.H. Holm, *Inorg. Chem.*, *31* (1992) 4778.
[48] J.-C. Gabriel, K. Boubekeur and P. Batail, *Inorg. Chem.*, 32 (1993) 2894.
[49] C. Brosset, *Ark. Kemi, Miner. Geol.*, *20A* (1945).
[50] C. Brosset, *Ark. Kemi, Miner. Geol.*, *22A* (1946).
[51] C. Brosset, *Ark. Kemi*, *1* (1949).
[52] P.A. Vaughan, *Proc. Natl. Acad. Sci. USA*, *36* (1950) 461.
[53] P. Nanelli and B.P. Block, *Inorg. Chem.*, *7* (1968) 2423.
[54] P.A. Vaughan, J.H. Sturtivant and L. Pauling, *J. Am. Chem. Soc.*, *72* (1950) 5477.
[55] H.S. Harned, C. Pauling and R.B. Corey, *J. Am. Chem. Soc.*, *82* (1960) 4815.
[56] R.J. Allen and J.C. Sheldon, *Aust. J. Chem.*, *18* (1964) 277.
[57] R.A. Mackay and R.F. Schneider, *Inorg. Chem.*, *6* (1967) 549.
[58] P.B. Fleming, T.A. Dougherty and R.E. McCarley, *J. Am. Chem. Soc.*, *89* (1967) 159.
[59] V.B. Spreckelmeyer, *Z. Anorg. Allg. Chem.*, *365* (1969) 225.
[60] P. B. Fleming and R.E. McCarley, *Inorg. Chem.*, *9* (1970) 1347.
[61] W. Geilmann and F.W. Wrigge, *Z. Anorg. Allg. Chem.*, *223* (1935) 144.
[62] M. Irmler and G. Meyer, *Z. Anorg. Allg. Chem.*, *552* (1987) 81.
[63] M. Irmler and G. Meyer, *Z. Anorg. Allg. Chem.*, *581* (1990) 104.
[64] F.A. Cotton and R.A. Walton, *Multiple Bonds Between Metal Atoms*, Oxford University Press, New York, 1993, 2nd edn.
[65] J. Zhang, R.P. Ziebarth and J.D. Corbett, *Inorg Chem.*, *31* (1992) 614.
[66] R.P. Ziebarth and J.D. Corbett, *J. Am. Chem. Soc.*, *107* (1985) 4571.
[67] R.P. Ziebarth and J.D. Corbett, *Inorg. Chem.*, *28* (1989) 626.
[68] R.P. Ziebarth and J.D. Corbett, *J. Solid State Chem.*, *80* (1989) 56.
[69] R.P. Ziebarth and J.D. Corbett, *J. Am. Chem. Soc.*, *110* (1988) 1132.
[70] R.P. Ziebarth and J.D. Corbett, *J. Am. Chem. Soc.*, *109* (1987) 4844.
[71] R.P. Ziebarth and J.D. Corbett, *J. Less-Common Met.*, *137* (1988) 21.
[72] J.D. Smith and J.D. Corbett, *J. Am. Chem. Soc.*, *108* (1986) 1927.
[73] R.P. Ziebarth and J.D. Corbett, *J. Am. Chem. Soc.*, *111* (1989) 3272.
[74] J.D. Smith and J.D. Corbett, *J. Am. Chem. Soc.*, *107* (1985) 5704.
[75] G. Rosenthal and J.D. Corbett, *Inorg. Chem.*, *27* (1988) 53.
[76] J. Zhang and J.D. Corbett, *Inorg. Chem.*, *30* (1991) 431.
[77] F. Rogel and J.D. Corbett, *J. Am. Chem. Soc.*, *112* (1990) 8198.
[78] F. Rogel, *PhD*, Iowa State University, 1990.
[79] H.L. Chum and R. Osteryoung, in D. Inman and D.G. Lovering (eds.), *Ionic Liquids*, Plenum, New York, 1981.
[80] R.J. Gale and R.A. Osteryoung, in D.G. Lovering and R.J. Gale (eds.), *Molten Salt Techniques*, Plenum, New York, 1983.
[81] C.L. Hussey, in G. Mamantov (ed.), *Advances in Molten Salt Chemistry*, Elsevier, Amsterdam, 1983.
[82] R.T. Carlin and J.S. Wilkes, in G. Mamantov and A.I. Popov (eds.), *Chemistry of Nonaqueous Solutions*, VCH, New York, 1994.
[83] C.L. Hussey, in G. Mamantov and A.I. Popov (eds.), *Chemistry of Nonaqueous Solutions*, VCH, New York, 1994.
[84] J.S. Wilks, J.A. Levisky, R.A. Wilson and C.L. Hussey, *Inorg. Chem.*, *21* (1982) 1263.
[85] A.A. Fannin, Jr., D.A. Floreani, L.A. King, J.S. Landers, B.J. Piersma, D.J. Stech, R.L. Vaughn, J.S. Wilkes and J.L. Williams, *J. Phys. Chem.*, *88* (1984) 2614.
[86] D. Appleby, C.L. Hussey, K.R. Seddon and J.E. Turp, *Nature*, *323* (1986) 614.
[87] C.L. Hussey, *Pure Appl. Chem.*, *60* (1988) 1763.
[88] S.K.D. Strubinger, I.-W. Sun, W.E. Cleland, Jr., and C.L. Hussey, *Inorg. Chem.*, *29* (1990) 993.
[89] S.K.D. Strubinger, I.-W. Sun, W.E. Cleland, Jr., and C.L. Hussey, *Inorg. Chem.*, *29* (1990) 4246.
[90] R.T. Carlin and R.A. Osteryoung, *Inorg. Chem.*, *27* (1987) 1482.
[91] P.A. Barnard, I.-W. Sun and C.L. Hussey, *Inorg. Chem.*, *29* (1990) 3670.
[92] S.K.D. Strubinger, C.L. Hussey and W.E. Cleland, Jr., *Inorg. Chem.*, *30* (1991) 4276.

[93] R. Quigley, P.A. Barnard, C.L. Hussey and K.R. Seddon, *Inorg. Chem.*, *31* (1992) 1255.
[94] M.R. Bond and T. Hughbanks, *Inorg. Chem.*, *31* (1992) 5015.
[95] C.E. Runyan, Jr., and T. Hughbanks, *J. Am. Chem. Soc.*, *116* (1994) 7909.
[96] C.E. Housecroft, D.M. Matthews, A. Waller, A.J. Edwards and A.L. Rheingold, *J. Chem. Soc., Dalton Trans.*, (1993) 3059.
[97] T.P. Fehlner, P.T. Czeck and R.F. Fenske, *Inorg. Chem.*, *29* (1990) 3103.
[98] N.P. Rath and T.P. Fehlner, *J. Am. Chem. Soc.*, *110* (1988) 5345.
[99] R. Khatter, J. Puga, T.P. Fehlner and A.L. Rheingold, *J. Am. Chem. Soc.*, *111* (1989) 1877.
[100] F.-E. Hong, T.J. Coffy, D.A. McCarthy and S.G. Shore, *Inorg. Chem.*, *28* (1989) 3284.
[101] K.S. Harpp, C.E. Housecroft, A.L. Rheingold and M.S. Shongwe, *J. Chem. Soc.*, *14* (1988) 965.
[102] C.E. Runyan, Jr., *Dissertation*, Texas A&M University, 1994.
[103] K.A. Yee and T. Hughbanks, *Inorg. Chem.*, *30* (1991) 2321.
[104] K.A. Yee and T. Hughbanks, *Inorg. Chem.*, *31* (1992) 1620.
[105] Y. Tian and T. Hughbanks, *Inorg. Chem.*, *32* (1993) 400.
[106] H.J. Mattausch, J.B. Hendricks, R. Eger, J. D. Corbett and A. Simon, *Inorg. Chem.*, *19* (1980) 2128.
[107] D.A. Lokken and J.D. Corbett, *Inorg. Chem.*, *12* (1973) 556.
[108] G. Ebbinghaus, A. Simon and A. Griffith, *Z. Naturforsch.*, *A37* (1982) 564.
[109] K. Ahn, T. Hughbanks, K.D.D. Rathnayaka and D.G. Naugle, *Chem. Mater.*, *6* (1994) 418.